PHILOSOPHICAL TRANSACTIONS A

rsta.royalsocietypublishing.org

Research

Article submitted to journal

Subject Areas:
Fracture, Crackling Dynamics, Scaling

Keywords:
Avalanches, Extreme Value Statistics, Depinning Transition

Author for correspondence:
S. Santucci
e-mail:
stephane.santucci@ens-lyon.fr

THE ROYAL SOCIETY PUBLISHING

Avalanches and extreme value statistics in interfacial crackling dynamics

S. Santucci[1,2,3], K. T. Tallakstad[2], L. Angheluta[2], L. Laurson[4,5], R. Toussaint[2,6] and K. J. Måløy[2]

[1]Université de Lyon, ENSL, UCBL, CNRS, Laboratoire de Physique, Lyon, France
[2]PoreLab,The Njord Center, Department of Physics, University of Oslo, Blindern, Oslo, Norway
[3]Lavrentyev Institute of Hydrodynamics, Novosibirsk, Russia
[4]Department of Applied Physics, Aalto University, P.O. Box 11100, FI-00076 Aalto, Espoo, Finland
[5]Laboratory of Physics, Tampere University of Technology, P.O. Box 692, FI-33101 Tampere, Finland
[6]Institut de Physique du Globe de Strasbourg, UMR 7516 CNRS, Université de Strasbourg, France

We study the avalanche and extreme statistics of the global velocity of a crack front, propagating slowly along a weak heterogeneous interface of a transparent PMMA block. The different loading conditions used (imposed constant velocity or creep relaxation) lead to a broad range of average crack front velocities. Our high-resolution and large data set allows to characterize in detail the observed intermittent crackling dynamics. We specifically measure the size S, the duration D, as well as the maximum amplitude V_{max} of the global avalanches, defined as bursts in the interfacial crack global velocity time series. Those quantities characterizing the crackling dynamics follow robust power-law distributions, with scaling exponents in agreement with the values predicted and obtained in numerical simulations of the critical depinning of a long-range elastic string, slowly driven in a random medium. Nevertheless, our experimental results also set the limit of such model which cannot reproduce the power-law distribution of the maximum amplitudes of avalanches of a given duration - reminiscent of the underlying fat-tail statistics of the local crack front velocities.

1. Introduction

The mechanical response of heterogeneous materials submitted to simple loading can present a complex behavior, in the form of collective excitations, bursts, with very broad size distributions usually following power-laws, separated by periods of rest, also broadly distributed [1]. This complexity culminates for instance, when considering faults dynamics during earthquakes, where slowly accumulated energy during the very slow motion of tectonic plates is suddenly released and dissipated by failure and frictional processes. The corresponding intermittent "crackling noises" [2] recorded by seismologists have indeed specific statistical characteristics, with for instance the famous scale-free Gutenberg-Richter law [3], relating the magnitude and total number of earthquakes, as well as, temporal correlations with aftershocks sequences following Omori's scaling law [4].

Such physical behavior is a common feature of numerous systems covering a broad range of scales, when compressing, or elongating laboratory heterogeneous samples like paper [5–7], wood [8], rocks [9], porous materials [10] and artificial rocks made of sintered polystyrene beads [11], or weakly sintered plexiglas plates [12–16]. Nevertheless, this phenomenology is not limited to the physical processes of deformation and rupture of disordered materials. Indeed, such intermittent avalanche dynamics can be observed for very different heterogeneous systems, slowly driven in out-of-equilibrium conditions, with for instance, the magnetic response of a disordered ferromagnet, also known as "Barkhausen Noise" [17,18], the vortex lines motion in superconductors [19], the fluid imbibition in porous and fractured media [20–23], the motion of contact lines over substrates with wetting heterogeneities [24], but also the yielding of amorphous materials [25–27] and single crystals [28–30] or even in the biological activity of neuronal networks [31,32] and cell migration [33].

Understanding the morphology and dynamics of interfaces slowly driven in disordered media has thus become a real challenge over the last thirty years. The common point of the so-called "Disordered Elastic Systems" [34] is the competition between the medium heterogeneities, which deform the fronts, while the elasticity of the system tends to maintain an orderly structure, and to smooth the interfaces. Those competing forces act at different spatial and temporal scales, leading indeed to complex structural and dynamical properties of the interfaces, with self-affine roughening morphologies and intermittent scale-free burst dynamics. Since the very first theoretical descriptions of the propagation of interfaces in random media [35,36], much progress has been achieved in last years, both theoretically and experimentally.

From a theoretical perspective, the detailed description of these systems is difficult and requires sophisticated approaches from nonlinear statistical physics [37,38]. Nevertheless, their critical-like scaling behavior could be interpreted in terms of non-equilibrium phase transitions [42], separating quiescent and active phases. Close to such dynamical phase transitions, the temporal fluctuations of an activity signal (as for instance, an interfacial velocity) acting as an order parameter display power-law scaling avalanches [1]. Statistical analyses and functional renormalization group calculations have succeeded to predict avalanche scaling exponents, within the mean field approximation and even beyond [38–41], and suggest to classify those systems displaying avalanche dynamics into "universality classes", characterized by their critical scaling exponents, directly related to the spatial dimension and the interaction range of the system, but a-priori independent of the microscopic material properties.

Thanks to experimental efforts to design model systems [12,21,43,44], where the structure and dynamics of interfaces could be directly observed and tracked very accurately both in space and time at the microscopic scale of the disorder, recent studies have been able to reconcile theoretical predictions and experimental observations. Specifically, it has been shown that both the structure and dynamics of planar cracks could be described quantitatively, at scales larger than the disorder, within the framework of a "critical depinining transition" [15,16,45–48].

In the present work, we describe novel experimental results obtained for such a model system, that allows to access the structure and the dynamics of an interfacial crack, propagating along

a weak disordered interface, locally at the scale of the heterogeneities. Usually, such spatial resolution is difficult to obtain, and the avalanche dynamics is typically studied only through the temporal evolution of a global, spatially-averaged quantity - also called "Crackling Noise". In contrast, our experimental set-up allows to bridge this gap, from local to global dynamics [49].

We present here an analysis of the avalanche and extreme statistics of the *global* velocity of a planar crack front, propagating slowly along a weak heterogeneous interface within a polymethyl methacrylate (PMMA) block. This *global* velocity is obtained from the spatial average of the front velocity measured at local microscopic scales, below the scale of heterogeneities. The originality of our study is indeed to analyze the crackling dynamics at a *global* scale, characterizing the statistics of *global* avalanches, extracted from the spatially-averaged crack front speed, while most of our previous studies on crack front avalanches have focused on local bursts, *e.g.* clusters of high local crack front velocity [12–14]. Moreover, in contrast with the more recent works reported in [15,16] (that focused on the avalanche shape and on the waiting time between subsequent avalanches, respectively), different loading conditions were used here. We thus could obtain a very high-resolution large data set, with in particular a broad range of average crack front velocities, spanning close to five decades, allowing us to characterize in detail the crackling dynamics. Indeed, we quantify the avalanche crack front dynamics by measuring the size and duration of global bursts in this crackling noise signal, *e.g.* the *global* crack front velocity. We show that our results are in quantitative agreement with previous theoretical and numerical results [15,46,48], with power-law exponents characterizing the size $\tau = 1.15 \pm 0.15$, and duration $\alpha = 1.32 \pm 0.15$ of those global avalanches, as well as their scaling $\langle D|S\rangle \sim S^{\xi}$ with $\xi = 0.60 \pm 0.15$. We thus confirm that the planar crack front avalanche dynamics at large scales can be well-described by the critical depinning of a long-range elastic string in a 2D random medium.

Furthermore, we have computed the extreme statistics of the velocity fluctuations corresponding to global avalanches. We find that the maximum avalanche velocity follows a power-law tailed distribution $P(V_{max}) \sim V_{max}^{-\epsilon}$ with an exponent $\epsilon = 1.34 \pm 0.15$. The average maximum velocity also scales with the avalanche duration as $\langle V_{max}|D\rangle \sim D^{\beta}$, with the exponent $\beta = 0.90 \pm 0.20$ that is also related by the scaling relation to the exponents of the avalanche duration and maximum amplitude distribution, namely $\epsilon = 1 + (\alpha - 1)/\beta$. We notice that the values of these exponents are different than those predicted from the mean-field theory of interface depinning [52,53], but the scaling relation between them is still valid. We observe nevertheless a quantitative agreement between the experimental values and those obtained from numerical simulations of a long-range elastic interface slowly driven along a disordered plane, beyond the mean-field approximation. However, there are also fundamental differences when comparing the scaling functions for the distribution of maximal velocities within avalanches of fixed duration. Albeit the mean values are in agreement with simulations, we find that maximal velocities are broadly varying with a tail-distribution that is similar to that of the local crack front velocity distribution and in particular its fat-tail $P(v) \sim v^{-\eta}$ with $\eta \sim 2.8$. This is not captured by the interfacial model which gives an exponential tail. Therefore, it can question the validity of the elastic line approach to describe the crack front dynamics at small scales close to the disorder, for which, a percolation-like approach [54,55] might be more relevant.

2. Experiments & Methods

We will first recall briefly the experimental set-up together with the samples preparation and methods of analysis, described in detail in [14,56].

Our samples consist of two sand-blasted Plexiglas plates that are annealed together to create a single block with a weak heterogeneous interface. Those plates have the following dimensions $(30, 14, 1)$ cm for the top (thicker and wider) one, and $(30, 12, 0.4)$ cm for the bottom one. Before annealing at a controlled temperature of $205\,^{\circ}$C for $30 - 50$ min, both plates are blasted on one side with $50\mu m$ steel particles or $100\mu m$ glass beads. Such procedure roughens the Plexiglas plates surfaces with a random topography which induces random toughness fluctuations at microscopic scales (few tenths of microns) during the annealing procedure [12]. A cylindrical

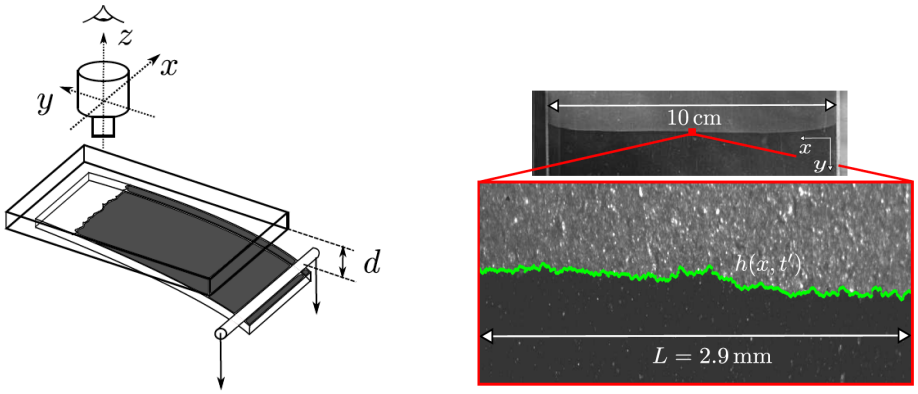

Figure 1. Left: Sketch of the experimental setup. Two initially sand-blasted and sintered PMMA plates create a weak heterogeneous interface, where a fracture – initiated by lowering a cylindrical press bar onto the lower plate – propagates. The fracture front is imaged from above by a high-resolution fast camera mounted on a microscope. Right: Typical fracture front $h(x, t')$ extracted at some time t' superimposed on the corresponding raw image, propagating from top to bottom. The framed raw image corresponds to a tiny central part of the full sample.

press bar mounted on a motorized vertical translation stage imposes a normal displacement to the thin plexiglas bottom plate, while the upper one is fixed to a rigid aluminum frame. Subsequently, a fracture propagates along the weak heterogenous plane between the sintered plates, in mixed mode I/II conditions, due to the unequal thickness of the two plates, and the loading asymmetry conditions (see Appendix in [56] for more details). Different loading conditions have been used, by either pushing the bottom plate at a constant velocity, *constant velocity boundary conditions* (F), or by imposing a constant deflection d to the bottom plate, *creep boundary conditions* (R).

A high-resolution and fast digital camera mounted on a microscope images a small central region of the crack front at the millimetre scale, as shown in Figure 1. The large width of the bent PMMA plate (10 cm) ensures that this central region of interest is not influenced by finite size effects. The sandblasting procedure – crucial to introduce toughness fluctuations along the weak plane – leads moreover to a very good contrast between the cracked and uncracked part of the sample, allowing to detect and extract rather easily the fracture font as shown in the bottom panel of Figure 1. For a more detailed description of the front extraction and image treatment, see [13]. The interfacial crack front propagation is captured with a high frame rate (from 1 fps to 2000 fps) compared to the average crack front velocity (typically 2 orders of magnitude faster), recording between 12 000 and 30 000 frames, using either a *Photron Fastcam-Ultima APX* (512×1024 pixels) or a *Pixelink Industrial Vision PL-A781* (2200×3000 pixels), at a spatial resolution $\sim 1 - 10\,\mu$m/pixel. We have performed various experiments with different loading conditions, leading to average crack front velocity spanning a very broad range (5 orders of magnitude). Indeed, our experiments could last few seconds to several hours, whereas the average distance of front propagation, is $\sim 500\,\mu$m in all cases.

The spatially random toughness fluctuations (induced by the sandblasting procedure) along the weak interface of the plexiglass block leads to a rough fracture front with complex self-affine scaling properties [45,47], and an intermittent avalanche dynamics [12] In order to characterize this jerky front propagation, we have developed an original procedure [12], based on the measurement of the local waiting time fluctuations of the crack front during its propagation. Such method has been successfully applied to quantify the avalanche dynamics of various systems, such as fluid imbibition fronts [57,58] or biological cells migration [33]. Specifically, we first computed the local front velocities $v(x, y)$ from measurements of the local waiting times $wt(x, y)$ elapsed while the crack front was located at a given position (x, y), and defining

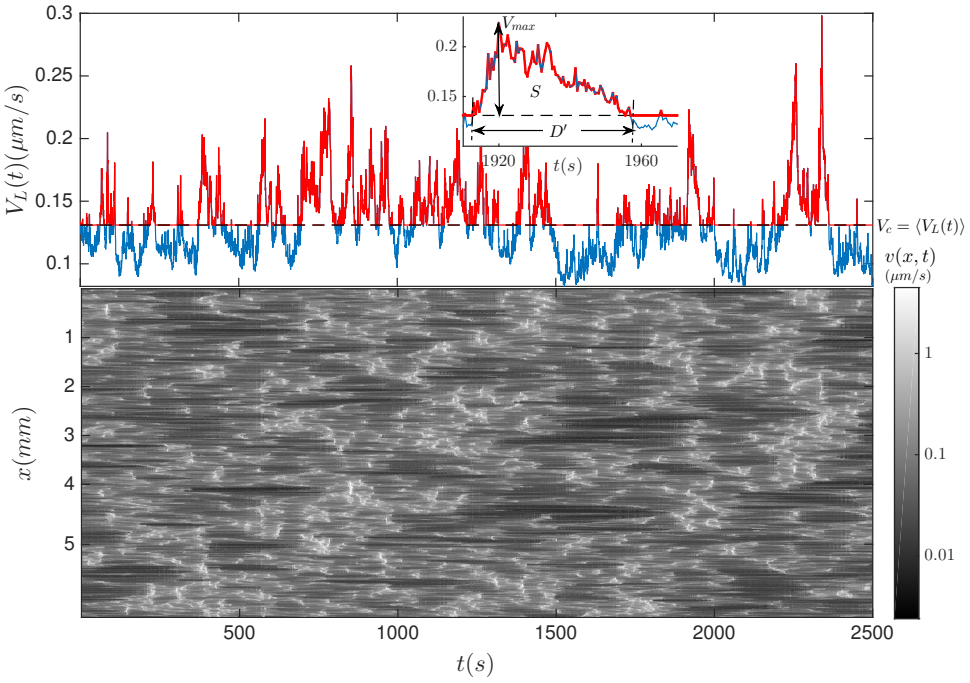

Figure 2. The bottom panel displays a typical spatio-temporal local velocity field $v(x,t)$ of the interfacial fracture during a slow creep experiment, which reflects the intermittent dynamics over a broad range of scales. In the top panel, the corresponding global velocity of the front $V_L(t) = \langle v(x,t) \rangle_L$, obtained from the local velocity field spatially averaged, here, at the scale L of the system size (e.g. image size) The dashed line indicates the threshold V_c used to define the global avalanches, of size S, duration D and of maximum velocity V_{max}, as explained in inset. Here, the threshold is equal to the total average front velocity. The size equals the area under connected points in $V_L(t)$ above the threshold line. For a given avalanche, the duration is the time difference between the two subsequent intersections with the threshold line. The maximum velocity is the peak value inside an avalanche minus the threshold velocity V_c.

$v(x,y) = r/wt(x,y)$, where r is the pixel resolution. Using the detected crack front position, $h(x,t)$ it is straightforward to obtain the spatio-temporal local velocity map $v(x,t)$, and the total average front velocity $\langle v \rangle = \langle v(x,t) \rangle_{x,t}$ of the fracture. Finally, from this local velocity field $v(x,t)$, we compute the spatially-averaged front velocity $V_l(t)$ over a variable window size $l \in (r, L)$, namely as $V_l(t) = \langle v(x,t) \rangle_{x_0}$ where the brackets correspond to an average of the local velocity over the abscissa x_0 of a window of size l. We have systematically varied the scale $l = L/N$ at which we measure the global velocity $V_l(t)$, obtaining finally N different crackling signals from one experiment with a crack length L. This window size l is always larger than the correlation length of the local velocities along the crack front, measured around 100 μm for our samples.

Figure 2 (top) shows the global velocity $V_L(t)$ for one typical creep experiment. This signal is obtained from the spatio-temporal local velocity map $v(x,t)$, spatially averaged at the scale L of the recorded images. This grey scale map illustrates the intermittent crack front dynamics. In particular, it has been shown previously that the front dynamics is governed by local avalanches – connected clusters of high local velocity – with very large size and velocity fluctuations following a fat-tail distribution $P(v) \sim v^{-\eta}$, decaying with a power law exponent $\eta \sim 2.7$. Consequently, the global crackling noise $V_l(t)$ signal follows a non-Gaussian statistics and, by the generalized central limit theorem, converges to a Levy-distribution [49] at large measuring scales l.

Here, we go further by studying the avalanche and extreme statistics of those global velocity fluctuations $V_l(t)$. Similar to earlier works [17,18,21,46], we introduce the concept of *global*

avalanches in the crack velocity signal. Each avalanche is characterized by its size S, duration D', and maximum amplitude V_{max} for a given threshold level $V_c = \langle v \rangle + C \cdot \sigma$, where C is a constant and σ corresponds to the standard deviation of the crack velocity signal $V_l(t)$:

$$D'_l = |t_b - t_a|, \text{ whenever } \begin{cases} V_l(t_a) = V_c \\ V_l(t_b) = V_c \\ V_l(t_a < t < t_b) > V_c \end{cases} \tag{2.1}$$

$$S_l = \int_{t_a}^{t_b} (V_l(t) - V_c)\, dt \tag{2.2}$$

$$V_{l,\max} = \max[V_l(t)]_{t\in(t_a,t_b)} - V_c\ . \tag{2.3}$$

The dimension of the global avalanche size S is a length, and it corresponds to the extra displacement of the fracture front in comparison to the global advancement of the crack at the velocity equals to the threshold value V_c, during the avalanche duration D'. In order to compare the duration statistics from experiments with very different average velocity $\langle v \rangle$, we compute the normalized duration D as $D = D'/D_0$, where $D_0 = r/\langle v \rangle$.

3. Avalanches and Extreme Values Statistics

Figure 3 shows the size and duration distribution $P(S)$ and $P(D)$ of the global avalanche for one given fracture experiment. The avalanches were computed from crackling signals $V_l(t)$ computed at various scales $l = L/N$, with $N = [1, 2, 4, 6, 8, 10, 12, 16, 20]$, while the threshold value was fixed using $C = -0.1$. We observe power-law distributions with exponential cut-offs, both for the size

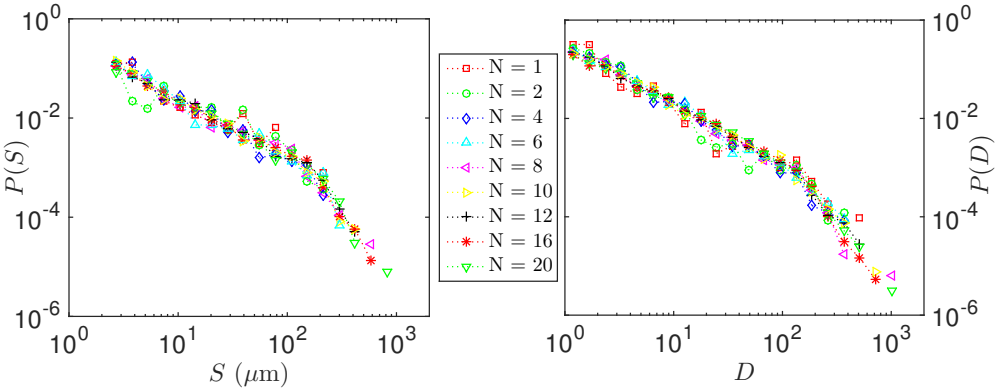

Figure 3. Probability distributions functions of the size S and normalized duration D of global avalanches computed from crackling noise signals measured at various length scales $l = L/N$, with $N = [1, 2, 4, 6, 8, 10, 12, 16, 20]$, from a single fracture experiment. The global avalanches are detected with a threshold level $C = -0.1$.

S and duration D. Interestingly, the distributions do not depend on the scale l at which the global quantity $V_l(t)$ is measured (as soon as l is larger than the correlation length scale of the local crack front velocities around 100 μm). Nevertheless, obviously, the statistics drastically improves as l decreases, since the number of crackling signals and thus the number of avalanches detected increases. We have previously reported that the local dynamics of the fracture front does not depend on the average front velocity, for either creep or constant velocity loading conditions [14]. Therefore, we expect a similar behavior for the global crackling noise signal $V_l(t)$.

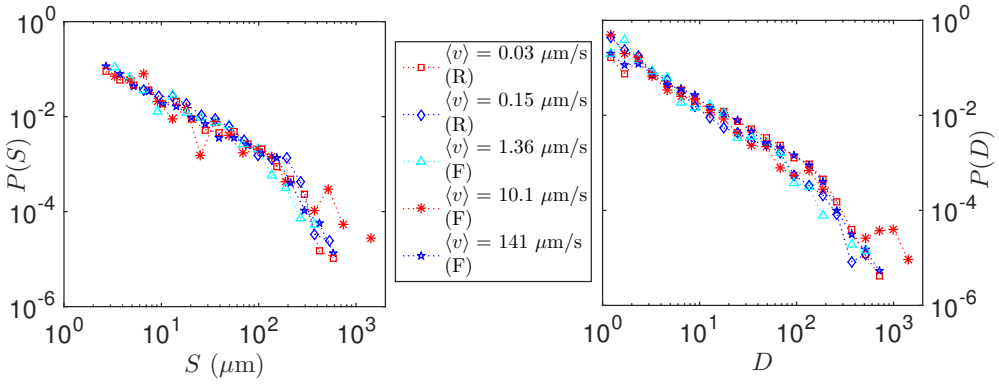

Figure 4. Probability distributions functions of the size S and normalized duration D of global avalanches detected for five different experiments, performed in different conditions leading to very different average crack front velocity, from around 0.02 to 150 μm/s. The global velocity is measured at a length scale $l = L/16$ and for a threshold level with $C = -0.1$.

In Figure 4, we represent the probability distribution functions of the size S and normalized duration D of global avalanches, detected for the global velocity of the crack front, measured at a length scale $l = L/N$, with $N = 16$ for a threshold level $C = -0.1$ for 5 experiments with very different average velocities, from around 0.02 to 150 μm/s (obtained in different loading conditions). Indeed, we can observe that those distributions – power-law up to an exponential cut-off – do not depend on the average crack front velocity. Moreover, we have also checked that we can obtain similar collapses for other values of N and C.

Therefore, we are then justified to accumulate statistics from all our experiments, with very different average front velocities. Moreover, we can also increase the statistics by computing, for each experiment, $N = 16$ different crackling noise signals, averaged velocity $V_l(t)$ measured at length scales $l = L/16$, as done previously in Fig. 4. This is valuable in order to find reliable scaling exponents and, to characterize precisely the distribution cut-offs and their dependence on the threshold value, which is exactly the goal of the analysis shown in the following figures. Indeed, we display the size and duration distributions of the global avalanches, changing systematically the threshold values $C \equiv [-0.3, -0.1, 0, 0.2, 0.5, 0.8, 1.2]$, in Figure 5. In the top-left figure, it is clear that the size distributions of the global avalanches $P(S)$ can be well fitted by a power law with an exponential cutoff S^* (represented by dashed black lines). For the range of thresholds used, we observe that the power-law exponent doesn't evolve, while the cut-off S^*decreases systematically as the threshold increases: $S^* = 128 c_r^{-1.9}$ with the normalized threshold velocity $c_r = V_c/\langle v\rangle = 1 + C\sigma/\langle v\rangle$. A similar scaling behavior is observed for the avalanches duration distributions (top-right) with the cut-off $D^* = 68 c_r^{-3.0}$. Therefore, we could use the values of those cut-offs to collapse the various distributions $P(S)$ and $P(D)$ allowing to extract reliable power-law exponents as shown at the bottom of Fig. 5,

$$P(S) \sim S^{-\tau}, \quad \text{with} \quad \tau = 1.15 \pm 0.15, \tag{3.1}$$

$$P(D) \sim D^{-\alpha}, \quad \text{with} \quad \alpha = 1.32 \pm 0.15. \tag{3.2}$$

Moreover, we also show (inset, bottom right figure 5) that the average avalanche duration of the global avalanches scales with the avalanche size as,

$$\langle D|S\rangle \sim S^{\xi}, \quad \text{with} \quad \xi = 0.60 \pm 0.15 \tag{3.3}$$

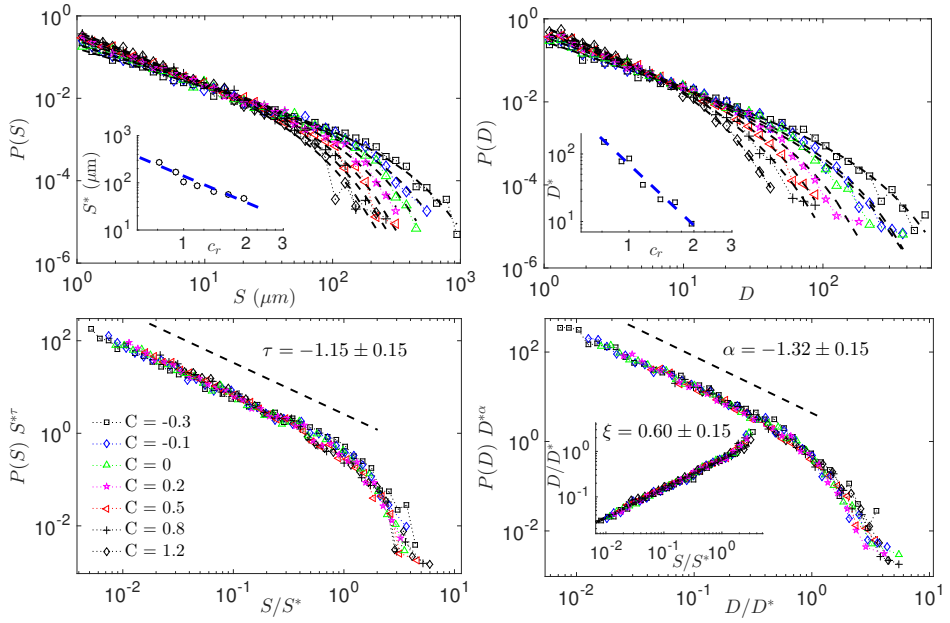

Figure 5. Distributions of avalanche sizes S (Top Left) and normalized durations D (Top Right), for various threshold values $C \equiv [-0.3, -0.1, 0, 0.2, 0.5, 0.8, 1.2]$, where the crackling noise signals have been measured at a scale $l = L/16$ (where L is the system size), for various experiments with a broad range of average crack front velocities (thanks to different loading conditions). Extracting the evolution of the exponential cut-off of each power-law distributions, S^* and D^*, for sizes and durations respectively (as shown in the top insets), we can collapse those distributions $P(S)$ and $P(D)$, when plotting $P(S)S^{*\tau}$ or $P(D)D^{*\alpha}$ as a function of rescaled observables S/S^* or D/D^*. The collapses displayed on the bottom figures allow us to extract reliable scaling exponents $\tau = 1.15 \pm 0.15$ and $\alpha = 1.32 \pm 0.15$. In the inset of the bottom right figure, we moreover show how the average avalanche duration scales with their average size, $\langle D|S\rangle \sim S^{\xi}$ with $\xi = 0.60 \pm 0.15$.

Those scaling exponents for the avalanche size and duration distributions are in remarkable agreement (within the rather large experimental error bars) with theoretical (using functional renormalization group calculations) and numerical predictions considering an interface with a long-range elasticity propagating in a random medium, giving $\tau = 1.25$, $\alpha = 1.43$, and $\xi = 0.58$ (see [15–17,46,48,50,51] and references therein). Moreover, it is important to notice that the values of those exponents characterizing the scaling behavior of the global avalanches are different when considering local crack front bursts [12,48]. Our new experimental results clearly confirm that high local velocity clusters and global avalanches measured on crackling time series are different observables with different statistical properties, as already reported in numerical simulations [46,48], and in imbibition experiments [23,57,58]. Finally, we can also remark that those scaling exponents are also different from those reported for a 3D crack front propagating in a bulk artificial rock [59]. This could suggest that the fracture of 3D solids may not be simply reduced to a 2D depinning problem. However, the scaling exponents reported in [59] evolve with the driving velocity, in strong contrast with our measurements, leading to robust scaling exponent values, for different loading conditions, with very different average crack front velocities. Therefore, this discrepancy might simply arise from the fact that the quasi-static assumption of the depinning model is not satisfied in those experiments.

To further characterize the statistics of these avalanches, we also examine their maximum amplitudes measured by V_{max}, where we have renormalized the crackling noise signal by the average crack front velocity value, i.e. $V_l(t)/\langle v\rangle$, to compare experiments performed at

very different average velocities. Figure 6 shows the distributions of the maximum amplitudes of avalanches measured for the same data set analyzed previously (figure 5), *e.g.* 5 different experiments with very different average crack front velocities, and for each experiments $N = 16$ different crackling noise signals (averaged velocity $V_l(t)$, measured at length scales $l = L/16$) were computed changing systematically the threshold values $C \equiv [-0.3, -0.1, 0, 0.2, 0.5, 0.8, 1.2]$. Strikingly, we observe that the distributions follow a power-law behavior with an exponential cut-off, independent of the threshold C,

$$P(V_{\max}) \sim V_{\max}^{-\epsilon}, \quad \text{with} \quad \epsilon = 1.34 \pm 0.15. \tag{3.4}$$

Moreover, in the inset of figure 6, we also show that the avalanche maximum velocities scales in average with the avalanche duration as,

$$\langle V_{max}|D\rangle \sim D^{\beta}\ , \quad \text{with} \quad \beta = 0.90 \pm 0.20 \tag{3.5}$$

Finally, using a simple change of variables, $P(V_{\max}) = P(D)|dD/dV_{\max}|$ we can relate those different scaling exponents, characterizing the statistics of the maximum amplitude of the global avalanche and their duration, as, $\epsilon = 1 + (\alpha - 1)/\beta$. Based on our previous measurements of α and β, we find $\epsilon \simeq 1.35$, which is consistent with our direct experimental measured value.

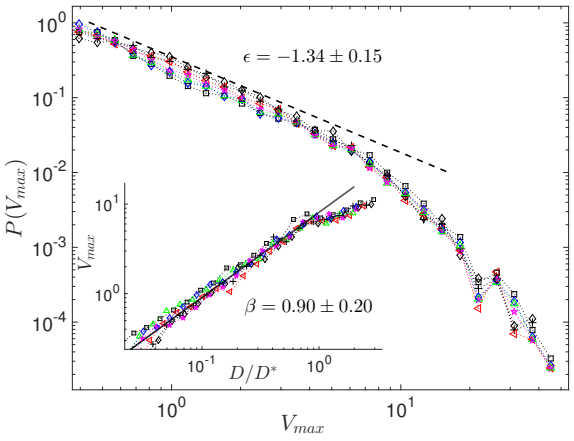

Figure 6. Distributions of the avalanche maximum velocities V_{max} for various threshold values $C \equiv [-0.3, -0.1, 0, 0.2, 0.5, 0.8, 1.2]$, for the same velocities time series $V_{L/16}(t)$ studied in fig 5. The inset gives the scaling of the average avalanche maximum velocities with the avalanche duration, $\langle V_{max}|D\rangle \sim D^{\beta}$, with $\beta \sim 0.90$.

It is interesting that the mean-field theory of interface depinning predicted a different exponent for the $P(V_{max}) \sim V_{max}^{-2}$ [52]. This is consistent with the other avalanche exponents that also deviate from the mean-field predictions. Additionally, the distribution of maximum amplitudes in avalanches of fixed durations was found to follow a scaling form $P(V_{max}|D) = \langle V_{max}|D\rangle^{-1}\mathcal{F}\left(V_{\max}/\langle V_{\max}|D\rangle\right)$, where the scaling function $\mathcal{F}(x)$ is determined analytically in terms of Bessel functions [53]. We find that a similar scaling form also holds beyond the mean field approximation, but with different expression for the scaling function $\mathcal{F}(x)$. Even though, it is difficult to extract clearly this scaling function from experimental measurements, we were able to compute $\mathcal{F}(x)$ from our large data set, obtained for different fracture experiments, driven at slow velocities of a few tenth of μm/s.

Figure 7, shows in inset the distributions $P(V_{\max}|D)$ of maximum velocities of avalanches of various fixed durations (chosen within the scaling range of the $\langle V_{\max}\rangle(D)$ relation shown in the inset of fig. 6); Those distributions can be collapsed by plotting $\langle V_{max}|D\rangle P(V_{max}|D)$ as a function

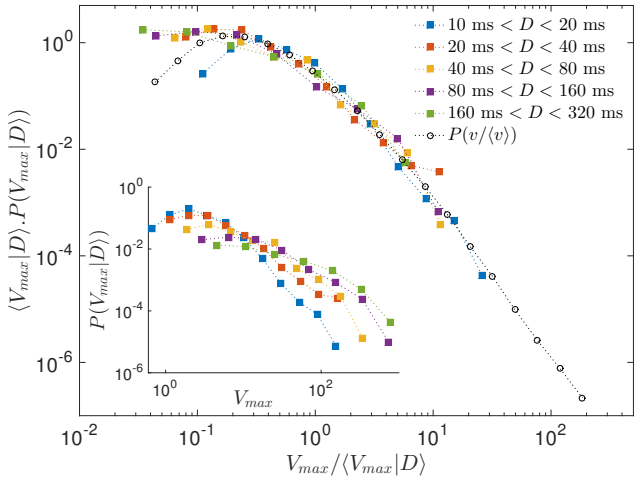

Figure 7. Distributions of maximum amplitudes V_{max} of global avalanches (detected with a clip level $C = 0$) $P(V_{\max}|D)$ for various fixed durations D-ranges (inset). The main panel demonstrates that these distributions can be collapsed as $P(V_{max}|D).\langle V_{max}|D\rangle = \mathcal{F}\left(V_{\max}/\langle V_{\max}|D\rangle\right)$. The scaling function $\mathcal{F}(x)$ is well described by the distribution of the corresponding local fracture front velocities $P(v/\langle v\rangle)$, displaying in particular a fat tail at large velocities $P(v) \sim v^{-2.8}$.

of the maximum amplitude of the global avalanches renormalized by their average amplitude $V_{\max}/\langle V_{\max}|D\rangle$, as shown in the main panel. The resulting scaling function $\mathcal{F}\left(V_{\max}/\langle V_{\max}|D\rangle\right)$ exhibits a power-law tail describing the largest maximum velocities $\mathcal{F}(x) \sim x^{-2.8}$, which - as expected - is very different from the mean-field prediction [52]. Interestingly, this scaling function and in particular its fat-tail, is similar to the distributions of the local front velocities $P(v/\langle v\rangle)$, plotted with black circles in the main panel of Fig. 7, at the origin of the non-gaussian Levy statistics of the global front velocity [49].

4. Numerical modeling of elastic interface depinning

Since the large scale avalanche dynamics of our planar crack seems to be well-described by the behavior of a long-range elastic string in a 2D random medium [15,48], we propose now to study the extremal statistics of the global avalanches, within the framework of such numerical model. So, here, we consider a discretized version of this line model, using periodic boundary conditions, with integer interface heights $h_i(t)$, $i = 1 \ldots L$, where L is the system size, and the lateral coordinates x_i of the interface are given by $x_i = i$. The total force acting on the interface element i is $F_i = \Gamma_0 \sum_{j \neq i} \frac{h_j - h_i}{|x_j - x_i|^2} + \eta(x_i, h_i) + F_{\text{ext}}$, where the long-range elastic interactions exhibit a $1/x^2$ decay along the interface, F_{ext} is the external driving force, and η is quenched spatially uncorrelated disorder describing toughness fluctuations of the disordered weak plane.

The crackling noise signal is given by $V(t) = 1/L \sum_i v_i(t)$, where $v_i = \theta(F_i)$, with θ the Heaviside step function; this implies that the local velocity at a given instant in time is either one (the interface is advancing locally) or zero (the interface is locally pinned). The interface is driven with a finite constant spatially averaged velocity $\langle V\rangle$, by imposing $F_{\text{ext}} = K(\langle V\rangle t - \langle h\rangle)$, where K describes the stiffness of the specimen-machine system and controls the cutoff avalanche size S^* and duration D^*, and $\langle h\rangle$ is the average interface height. We show here results for $L = 32768$ and a slow but finite driving velocity $\langle V\rangle = 4/32768$. We have checked that other small $\langle V\rangle$ values yield similar results. To define global avalanches and their maximum amplitude, we set the threshold

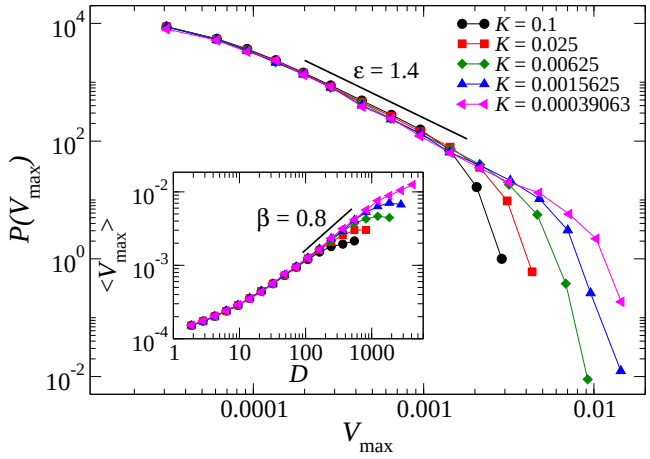

Figure 8. Main panel: Distributions $P(V_{\max})$ for various K, displaying a power law with $\epsilon = 1.4 \pm 0.1$, and a K-dependent cutoff. Inset: Scaling of $\langle V_{\max} \rangle$ with D, displaying a power-law with $\beta = 0.8 \pm 0.1$.

value to $V_c = \langle V \rangle$; in what follows, we denote by $V_{\max}$ the global maximum velocity of avalanches from which the threshold value V_c has been subtracted.

The main panel of Fig. 8 shows the scaling of the distributions $P(V_{\max})$ for all avalanches detected for different values of the stiffness parameter K. We observe a clear power-law behavior terminated at a K-dependent cut-off, with a power-law exponent $\epsilon = 1.4 \pm 0.1$, in quantitative agreement with our experimental measurements. The inset of Fig. 8 shows the scaling of $\langle V_{\max} \rangle$ with D, displaying again a power-law relation similar to the experimental one with $\beta = 0.8 \pm 0.1$. This scaling exponent is slightly smaller but still, in very good agreement within the large error bars with the one measured in our fracture experiments.

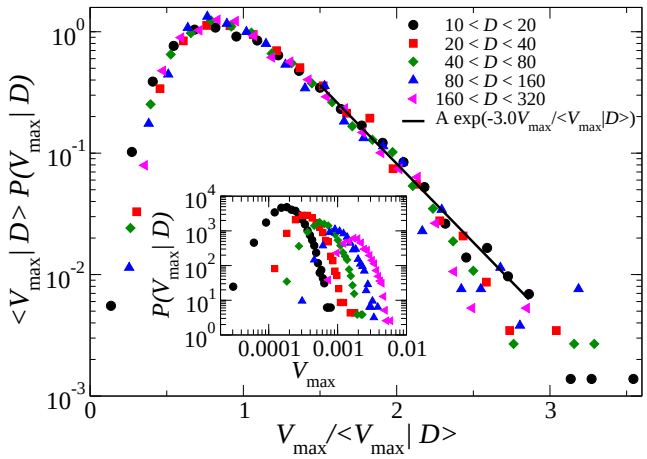

Figure 9. The inset shows the distributions $P(V_{\max}|D)$ at various fixed durations D-ranges. The main panel demonstrates that these distribution can be collapsed, when plotting $\langle V_{max}|D \rangle P(V_{max}|D)$ as a function of $V_{\max}/\langle V_{\max}|D \rangle$ in a semi-log scale. The scaling function has a clear exponential tail different from the power-law behavior of the experimental data.

We have also computed the distributions $P(V_{\max}|D)$ of the maximum amplitudes of avalanches for various fixed duration ranges D (taken within the scaling range of the $\langle V_{\max}\rangle(D)$ relation), as shown in the inset of Fig. 9. The main panel of this figure demonstrates that those distributions can be collapsed - as for our experimental data - by representing $\mathcal{F}(V_{\max}/\langle V_{\max}|D\rangle) = \langle V_{max}|D\rangle P(V_{max}|D)$ as a function of $V_{\max}/\langle V_{\max}|D\rangle$, in a semi-logarithmic plot. The resulting scaling function $\mathcal{F}$ exhibits a roughly exponential tail describing the largest maximum velocities. As expected, this scaling function has a different shape than the analytical prediction obtained within the mean-field approach [53]. Nevertheless, it is important to notice that this scaling function $\mathcal{F}$ is also different from the experimental one which displays a power-law tail instead of an exponential one.

Finally, considering the scaling form observed for the conditional distribution of maximal velocities within avalanches of duration D, $P(V_{\max}|D) = \langle V_{\max}|D\rangle^{-1}\mathcal{F}(V_{\max}/\langle V_{\max}|D\rangle)$ and the power-law distributions for the avalanche durations $P(D) \sim D^{-\alpha}$, we can show that the distribution of the maximum amplitudes of avalanches, $P(V_{\max}) = \int dD\, P(V_{\max}|D)P(D)$, using the change of integration variables $y = V_{\max}/\langle V_{\max}|D\rangle \sim V_{\max}/D^{\beta}$, can be written as :

$$P(V_{\max}) \sim V_{\max}^{-\epsilon} \int dy\, y^{\epsilon-1}\mathcal{F}(y), \quad \text{with } \epsilon = 1 + (\alpha-1)/\beta \tag{4.1}$$

Therefore, this formula shows that the scaling of $P(V_{\max})$ does not depend on the conditional distribution $P(V_{\max}|D)$ as long as the integral in eq. 4.1 converges; thus, it explains why we could observe the same "universal" power-law distributions for the maximum velocities considering all avalanches, $P(V_{\max}) \sim V_{\max}^{-\epsilon}$, between our experiments and numerical simulations (with a quantitative agreement), despite different underlying conditional distributions $P(V_{\max}|D)$.

5. Conclusion

We have presented an experimental study of the global, spatially averaged, velocity of an interfacial crack propagating along a weak disorder plane in a transparent PMMA block. This crackling noise signal is highly intermittent, with power-law distributed avalanches in size, duration and maximum amplitudes. We confirm that the critical depinning of a long-range elastic string propagating in a 2D disordered medium describes quantitatively the scaling behavior of most of our experimental observables. However, we could also show that such model fails to reproduce the power-law distribution of the maximum amplitude of avalanches at fixed duration, which may be the signature of the fat-tail power-law statistics of the local crack front velocity. A different approach describing material failure as a correlated percolation process considering crack coalescence [54,55] could lead to such largely power-law distributed local velocity of the crack front [12,14,49]. Therefore, our results suggest that different approaches may be needed to fully describe the intermittent crack front dynamics, as for its complex self-affine morphology [45,47,60]. While at larges scales, the long-range elastic line model appears very successful, different approaches such as a percolation-like model [54,55] or thermally-activated processes [61–63] could be more relevant to describe material failure at the local scale of the heterogeneities.

Data Accessibility. Experimental and numerical data are accessible upon reasonable request to the authors.

Authors' Contributions. All authors significantly contributed to this work as a team effort. SS, KJM, RT and LA designed the study. SS and KTT performed the experiments and its analysis. LL performed the numerical modeling and its analysis. All authors participated to the analysis, and interpretation of the data. SS wrote the manuscript firstly drafted by KTT and LA. All authors read, revised critically and approved the manuscript.

Competing Interests. The authors declare that they have no competing interests.

Funding. This work was supported by the Russian Government with Grant No. 14.W03.31.0002, the CNRS with the French/Norwegian International Associated Laboratory (LIA, "D-FFRACT"), and by the Academy of Finland through an Academy Research Fellowship (LL, project no. 268302). We also acknowledge the support of the University of Oslo and the support by the Research Council of Norway through its Centres of Excellence funding scheme, project number 262644, and through the Frinat Grant No. 205486.

References

1. D. S. Fisher, "Collective transport in random media: from superconductors to earthquakes", Physics Reports 301, 113150 (1998)
2. J. P. Sethna, K. Dahmen and C.R. Myers, Nature **410**, 242 (2001).
3. B. Gutenberg and C. F. Richter, Ann. Geofis., **9**,1-15 (1956).
4. F. Omori, J. College Sci., Imp. Univ. Tokyo, **7**, 111-200 (1894).
5. L. I. Salminen, A. I. Tolvanen, and M. J. Alava, Phys. Rev. Lett. **89**, 185503 (2002).
6. S. Santucci, L. Vanel, L and S. Ciliberto, Phys. Rev. Lett. **93**, 095505 (2004).
7. M. Stojanova, S. Santucci, L. Vanel, and O. Ramos, Phys. Rev. Lett. **112**, 115502 (2014).
8. T. Makinen, A. Miksic, M. Ovaska, and M. J. Alava, Phys. Rev. Lett. **115**, 055501 (2015).
9. J. Davidsen, S. Stanchits, and G. Dresen Phys. Rev. Lett. **98**, 125502 (2007)
10. J. Baró, A. Corral, X. Illa, A. Planes, E. K. H. Salje, W. Schranz, D. E. Soto-Parra, and E. Vives, Phys. Rev. Lett. **110**, 088702 (2013).
11. J. Barés, A. Dubois, L. Hattali, D. Dalmas, D. Bonamy, Nature Communications, **9**, 1253 (2018)
12. K. J. Måløy, S. Santucci, J. Schmittbuhl, and R. Toussaint Phys. Rev. Lett. **96**, 045501 (2006).
13. M. Grob, J. Schmittbuhl, R. Toussaint, L. Rivera, S. Santucci, and K. J. Måløy, Pure appl. geophys. **166**, 777 (2009).
14. K. T. Tallakstad, R. Toussaint, S. Santucci, J. Schmittbuhl, and K. J. Måløy, Physical Review E **83**, 046108 (2011)
15. L. Laurson, X. Illa, S. Santucci, K. T. Tallakstad, K. J. Måløy, and M. J. Alava, Nat. Commun. **4**, 2927 (2013).
16. S. Janićević, L. Laurson, K. J. Måløy, S. Santucci, and M. J. Alava, Phys. Rev. Lett. **117**, 230601 (2016).
17. S. Zapperi, P. Cizeau, G. Durin, H.E. Stanley Physical Review B **58** (10), 6353 (1998)
18. G. Durin and S. Zapperi, The Science of Hysteresis, edited by G. Bertotti and I. Mayergoyz (Academic Press, Amsterdam, 2006), pp. 181-267.
19. G. Blatter, M. V. Feigelman, V. B. Geshkenbein, A. I. Larkin, and V. M. Vinokur, Rev. Mod. Phys, **66**, 1125 (1994).
20. M. Rost, L. Laurson, M. Dubé, and M. J. Alava, Phys. Rev. Lett. **98**, 054502 (2007).
21. R. Planet, S. Santucci, and J. Ortín, Phys. Rev. Lett. **102**, 094502 (2009).
22. S. Santucci, R. Planet, K. J. Måløy, and J. Ortín, Europhys. Lett. **94**, 46005 (2011).
23. R. Planet, J. M. Lopez, S. Santucci, and J. Ortín, Phys. Rev. Lett. **121**, 034101 (2018).
24. A. Prevost, E. Rolley, and C. Guthmann, Phys. Rev. B **65**, 064517 (2002).
25. J. Lin, E. Lerner, A. Rosso and M. Wyart PNAS **111**, 14382 (2014)
26. J. Lin, T. Gueudré, A. Rosso, and M. Wyart Phys. Rev. Lett.**115**, 168001 (2015)
27. C. Liu, E. Ferrero, F. Puosi, J.-L. Barrat and K. Martens Phys. Rev. Lett. **116**, 065501 (2016)
28. M. C. Miguel, A. Vespignani, S. Zapperi, J. Weiss, and J. R. Grasso, Nature (London) 410, 667 (2001).
29. D. M. Dimiduk, C. Woodward, R. LeSar, and M. D. Uchic, Science 312, 1188 (2006).
30. M. D. Uchic, P. A. Shade, and D. M. Dimiduk, Annual Review of Materials Research **39**, 361 (2009).
31. J. G. Orlandi, J. Soriano, E. Alvarez-Lacalle, S. Teller and J. Casademunt Nature Physics, **9**, 582-590 (2013)
32. T. Bellay, A. Klaus, S. Seshadri, and D. Plenz, eLife **4**, e07224 (2015).
33. O. Chepizhko, et al, PNAS **113** , 41, 11408-11413 (2016)
34. T. Giamarchi, A. B. Kolton, A. Rosso "Dynamics of disordered elastic systems", Lecture Notes in Physics 688, 91 (2006)
35. S.F. Edwards, D.R. Wilkinson Proc. Roy. Soc. London Ser. A, 381, 17 (1982).
36. M. Kardar, G. Parisi, Y.-C. Zhang Phys. Rev. Lett., **56**, 889 (1986).
37. D. S. Fisher, Phys. Rev. Lett. **56**, 1964 (1986).
38. P. Le Doussal and K. J. Wiese, Phys. Rev. E **79**, 051106 (2009).
39. P. Le Doussal, and K. J. Wiese EPL **97** 46004 (2012)
40. P. Le Doussal, and K. J. Wiese Phys. Rev. E **88** 022106 (2013)
41. A. Dobrinevski, P. Le Doussal, and K. J. Wiese EPL **108** 66002 (2014)
42. S. Lubeck, Int. J. Mod. Phys. B **18**, 3977 (2004).
43. J. Schmittbuhl and K. J. Måløy, Phys. Rev. Lett. **78**, 3888 (1997).
44. J. Ortin, and S. Santucci, (2017) pp 261-292 *Avalanches, Non-Gaussian Fluctuations and Intermittency in Fluid Imbibition*, In: Salje E., Saxena A., Planes A. (eds) Avalanches in Functional Materials and Geophysics. Understanding Complex Systems. Springer, Cham

45. S. Santucci et al, Phys. Rev. E **75**, 016104 (2007)
46. D. Bonamy, S. Santucci and L. Ponson, Phys. Rev. Lett. **101**, 045501 (2008).
47. S. Santucci, M. Grob, R. Toussaint, J. Schmittbuhl, A. Hansen and K.J. Måløy, EPL **92**, 44001, (2010)
48. L. Laurson, S. Santucci, and S. Zapperi, Phys. Rev. E **81**, 046116 (2010).
49. K. T. Tallakstad, R. Toussaint, S. Santucci, and K.J. Måløy, Phys. Rev. Lett. **110**, 145501 (2013).
50. A. Tanguy, M. Gounelle, and S. Roux, Phys. Rev. E **58**, 1577 (1998).
51. P. Moretti, M. C. Miguel, M. Zaiser, and S. Zapperi, Phys. Rev. B **69**, 214103 (2004).
52. M. LeBlanc, L. Angheluta, K. Dahmen, and N. Goldenfeld, Physical Review E **87**, 022126 (2013).
53. M. LeBlanc, L. Angheluta, K. Dahmen, and N. Goldenfeld, Physical Review Letters **109**, 105702 (2012).
54. K. S. Gjerden, A. Stormo and A. Hansen Front. Phys. 2:66, (2014). doi: 10.3389/fphy.2014.00066
55. A. Stormo, O. Lengliné, J. Schmittbuhl and A. Hansen Front. Phys., 11 May (2016) https://doi.org/10.3389/fphy.2016.00018
56. O. Lengliné, R. Toussaint, J. Schmittbuhl, J. E. Elkhoury, J. P. Ampuero, K. T. Tallakstad, S. Santucci, and K.J. Måløy, Phys. Rev. E **84**, 036104 (2011)
57. X. Clotet, J. Ortín, and S. Santucci, Phys. Rev. E **93**, 012149 (2016)
58. X. Clotet, S. Santucci and J. Ortín, Phys. Rev. E **93**, 012150 (2016)
59. J. Barés, M. L. Hattali, D. Dalmas, and D. Bonamy, PRL **113**, 264301 (2014)
60. D. Bonamy, Journal of Physics D: Applied Physics **42**, 2114014 (2009)
61. S. Santucci, P.-P. Cortet, S. Deschanel, L. Vanel, S. Ciliberto, EPL, **74**, 4, 595-601 (2006)
62. S. Santucci, L. Vanel, S. Ciliberto, EPJ-ST, **146**, 341-356 (2007)
63. A. Cochard, O. Lengliné, K.J. Måløy and R. Toussaint, submitted to Phil. Trans. R. Soc. A (2018).